Available online at www.sciencedirect.com
SCIENCE DIRECT®
Journal of Catalysis 229 (2005) 513–524
JOURNAL OF CATALYSIS
www.elsevier.com/locate/jcat

Optimisation of olefin epoxidation catalysts with the application of high-throughput and genetic algorithms assisted by artificial neural networks (softcomputing techniques)

A. Corma [a,*], J.M. Serra [a], P. Serna [a], S. Valero [b], E. Argente [b], V. Botti [b]

[a] *Instituto de Tecnología Química, UPV, Av. Naranjos s/n, E-46022 Valencia, Spain*
[b] *Dept. Sistemas Informáticos y Computación, UPV, Av. Naranjos s/n, E-46022 Valencia, Spain*

Received 27 September 2004; revised 15 November 2004; accepted 16 November 2004
Available online 28 December 2004

Abstract

An olefin epoxidation Ti catalyst has been optimised by means of high-throughput experimentation involving materials synthesis, postsynthesis treatments, and catalytic testing. Softcomputing techniques for advanced experimental design have been used. The variables explored in the hydrothermal synthesis of Ti-silicate-based catalysts were: concentration of OH^-, titanium, and surfactant. The probe reaction employed for the optimisation was the solvent-free epoxidation of cyclohexene, with *tert*-butylhydroperoxide as oxidant. The different catalyst groups detected by clustering analysis were studied by XRD and UV diffuse reflectance. Ti-mesoporous MCM-41 and MCM-48 molecular sieves were among the most active catalysts. The best performing catalysts were tested for epoxidation of different linear olefins.

Keywords: Genetic algorithm; Neural networks; High-throughput; Epoxidation; Titanium; MCM-41; MCM-48

1. Introduction

The development of high-throughput experimental tools for materials synthesis, catalytic testing, and physicochemical characterisation has made it possible to explore simultaneously a large number of variables. The growth of those accelerated tools has been accompanied by the development of software techniques for data management, multivariable experimental design, and data mining. Such research that applies accelerated experimental tools combined with powerful computational techniques constitutes so-called combinatorial catalysis.

An important issue in catalytic experimentation is how to design the experiments in order to explore and optimise the multidimensional parameter space, minimising the number of trials required to achieve a unique solution. Approaches for experimental design include techniques like factorial designs [1], deterministic optimisation algorithms like holographic search [2] and *split & pool* methods [3,4], or stochastic procedures like simulated annealing and genetic algorithms (GAs). The most suitable procedure for multidimensional optimisation in the field of catalysis is genetic algorithms [5,6].

We have developed a new approach [7] for experimental design that involves the combination of data-mining techniques with high-dimensional optimisation algorithms, in such a way that the knowledge extracted from the previous experimentation can be applied in the design of the new subset of catalysts to be experimentally screened in the next optimisation step. One of those techniques comprises the combination of an artificial neural network (ANN) and a GA. Thus, whereas the ANN finds the internal relationships between catalyst variables in the data from the screening of the previous generations, the optimisation algorithm (GA) designs the next generation of catalysts to be screened, taking into account the knowledge extracted by the ANN. The com-

* Corresponding author.
E-mail address: acorma@itq.upv.es (A. Corma).

0021-9517/$ – see front matter
doi:10.1016/j.jcat.2004.11.024

bination of the two artificial intelligence techniques is now being widely applied [8–12]; this is called SoftComputing [13,14].

Metal-containing zeolites such as TS-1 [15,16], Ti-Beta [17], and Sn-Beta [18,19] are interesting Lewis acid catalysts for the oxidation of alcohols, olefins, alkanes, ketones, and aldehydes to esters (Baeyer–Villiger oxidation); hydroxylation of aromatics; and ammoxidation of ketones, with H_2O_2 as the oxidant.

An important breakthrough was the discovery of Ti-silicalite (TS-1). This material has isolated tetrahedrally coordinated titanium sites in the silicate framework and shows interesting catalytic properties due to its isolated Lewis acid sites [20]. The synthesis of other Ti-silicate materials like Ti-beta, Ti-MCM-41 [21,22], and Ti-MCM-48 [23–25] broadened the scope of these oxidation catalysts for the conversion of larger hydrocarbon molecules. It has been shown with these catalytic systems that the hydrophobic/hydrophilic properties of the surface are just as important as the number of active sites for catalysing the epoxidation of olefins [26]. Control of the hydrophobicity of the molecular sieve allows the optimisation of the adsorption of the olefin and products, reducing the adsorption of water and the polar epoxide over the surface silanol groups and over the =Ti–OH groups, reducing the formation of diols and the deactivation of the catalyst [27].

In this work, the synthesis variables of mesoporous Ti-silicate materials are intensively and simultaneously explored with the aim of optimising the catalytic performance of the resulting catalysts for the epoxidation of olefins. The materials were characterised by XRD, UV spectroscopy, SEM, and N_2 adsorption to establish relationships between the synthesis conditions and the nature of the Ti sites, the structure order, particle size, textural properties, and catalytic activity. This multivariable space has been shown to be a nonlinear space, and, therefore, we propose here to study simultaneously the effect of all synthesis variables on catalytic activity. To do this we have chosen high-throughput tools for synthesis and catalytic testing, and the design of experiments was directed by a novel artificial intelligence technique. Therefore, the optimisation procedure shown here could also serve as a model study using state-of-art combinatorial methodologies.

2. Experimental

2.1. Synthesis of Ti-silicate catalysts

Ti-silicates were synthesised by means of automated robotic equipment developed in-house. The preparation required three different steps: (1) synthesis of the gel, (2) crystallisation under hydrothermal conditions, and (3) postsynthesis treatment, including organic extraction, dehydration, and silylation. Ti samples were synthesised by a procedure described elsewhere [27,28]. Starting gel precursors were amorphous silica (Aerosil 200, Degussa), 25 wt% aqueous solution of tetramethylammonium hydroxide (Aldrich, 25 wt%), an aqueous solution of hexadecyltrimethylammonium bromide (CTMABr), titanium(IV) ethoxide (Alfa Aesar, 33% min), and CTMAOH, which was obtained from CTMABr by ionic exchange.

The starting gels were synthesised with a robotic system built in-house, which can automatically perform the following routines: (i) dosing of liquid and solid reagents, (ii) evaporation of solvents by IR heating under airflow, and (iii) gel homogenisation by vigorous stirring. For each sample, CTMAOH, CTMABr, and TMAOH, if required, were mixed according to the desired chemical composition until total homogenisation. Then, titanium ethoxide and silica were added. All gels obtained conformed to the following molar composition: x SiO_2, y $Ti(OEt)_4$, z CTMA, k TMA, 26 OH, H_2O. Crystallisation was carried out inside Teflon vials placed automatically in a 15-well stainless-steel rack. The Ti-silicates were synthesised at 408 K for 24 h. The maximum gel volume per individual synthesis was 3.5 ml, and the typical solid mass obtained after washing and drying ranged from 0.1 to 0.25 g, depending on the molar gel composition and the crystallisation yield.

Surfactant extraction and silylation [22,27] were performed with the use of a liquid-handling robot equipped with a stirring and heating station. Extraction was performed in two steps, first with a 0,05 M H_2SO_4–ethanol solution and afterwards with a 0,15 M HCl–ethanol/n-heptane (48/52) solution, under reflux at 363 K for 1 h in both cases. Extracted Ti-silicate samples were dehydrated under vacuum (10^{-2} bar, 433 K for 2 h) and silylated with hexamethyldisilazane in toluene under reflux (358 K for 2 h). The catalysts were filtered, washed with toluene, and dried at 333 K overnight, yielding catalyst amounts in the range of 20–150 mg.

Samples synthesised for this work were compared with a high-activity Ti-MCM-41 catalyst [27]. The gel molar composition of this reference catalyst is 0.015 SiO_2, 0.15 $Ti(OEt)_4$, 0.26 CTMA, 0.26 TMA, 24 OH, H_2O, and it was crystallised in a 60-ml lined-lined stainless steel autoclave at 373 K for 24 h under static conditions. Surfactant extraction and silylation were carried out with the procedure described above.

2.2. Catalytic testing

Reactions were carried out in 2-ml glass flasks with magnetic stirring and heated by means of a temperature-controlled aluminum rack (Fig. 1). The equipment allows high-throughput testing by processing 21 batch reactions in parallel. Aliquots were taken with an autosampler (Konic K-MAS5), and reaction products were analysed on-line by ultrafast gas chromatography (column HP5, 3 m length, analysis time 90 s). Together with the integration of the multibatch reactor and the autosampler, the ultrafast analysis system provided a large quantity of results that made it

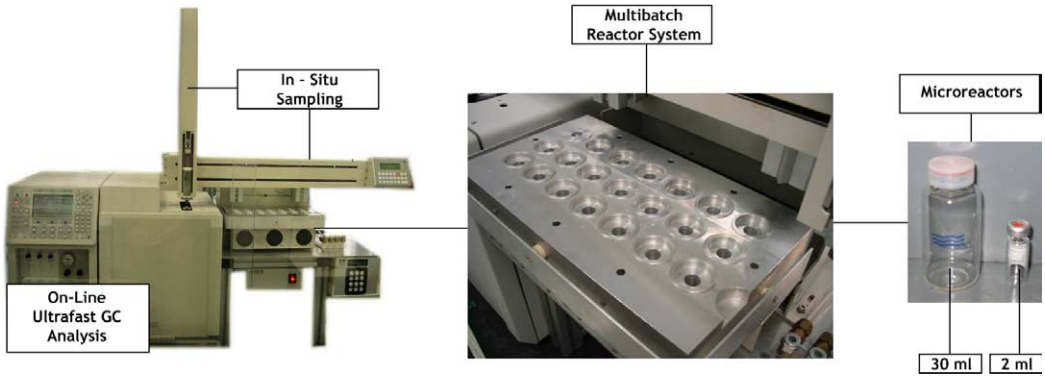

Fig. 1. Multibatch Automatic Reactor used for catalytic testing for olefin epoxidation. Sets of 21 reactions were studied simultaneously, using 2 ml glass flasks.

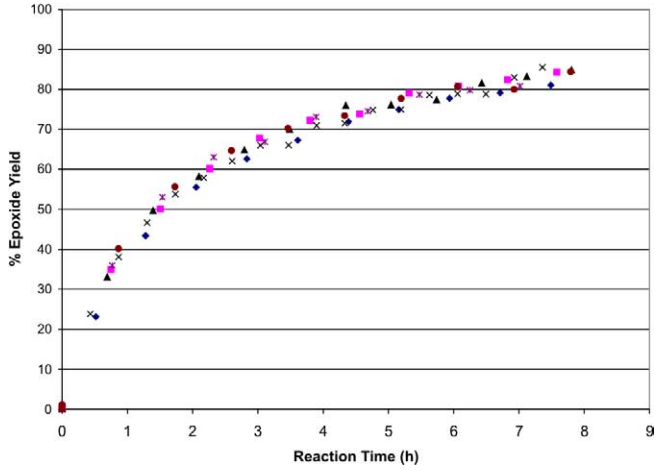

Reference catalyst (yield at 5 h) (%)
74.5
77.3
76.9
76.6
75.4
77.2

Standart deviation = 1.12.

Fig. 2. Epoxide yield evolution using the reference Ti-MCM-41 catalyst as reproducibility test (323 K; 785 mg of cyclohexene, 215 mg of TBHP and 5 mg of catalyst).

possible to follow the reaction with time and to carry out rigorous kinetic studies (Fig. 2).

The reaction probe employed for catalyst optimisation was the solvent-free epoxidation of cyclohexene with *tert*-butylhydroperoxide as the oxidant, under the following model reaction conditions. Experiments were done at 323 K and 333 K, with cyclohexene (Fluka > 98%) as the substrate and *tert*-butylhydroperoxide TBHP (Aldrich, 80% in di-*tert*-butylperoxide/water 3/2) as the oxidant. Reactions were performed with 785 mg of cyclohexene, 215 mg of TBHP (molar olefin/oxidant ratio = 4), 5 mg of catalyst (0.5 wt%), and 1.5 wt% water. The best performing catalysts were tested for epoxidation of different linear olefins such as 1-hexene (Fluka, 99.5%), 1-decene (Fluka, 98%), and 1-dodecene (Fluka, 98%). The reproducibility of catalytic tests was checked against a reference catalyst (extracted and silylated Ti-MCM-41). Fig. 2 shows a summary of the curves obtained with the reference catalyst in different runs. We tested the possibility of mass transfer control by automatically changing the stirring speed from 100 to 1000 rpm (external diffusion). It was found that at 300 rpm the process was not controlled by external diffusion. Internal diffusion limitation was avoided with catalyst particles with a diameters $\leqslant 0.1$ mm. Only experiments with a mass balance $\geqslant 95\%$ were considered.

2.3. Characterisation

X-ray powder was performed with a Philips X'Pert MPD diffractometer equipped with a PW3050 goniometer, with the use of Cu-K_α radiation and a multisample handler. DR UV–vis spectra were reordered with a Perkin Elmer (Lambda 19) spectrometer equipped with an integrating sphere, with $BaSO_4$ as a reference. The carbon content of silylated samples was quantified with a Fisons EA 1108CHN-S analyser. Particle size was measured by SEM (JEOL JSM-6300 microscope).

3. Experimental design by softcomputing techniques

The experimental design was carried out with the use of a hybrid algorithm we developed [7] (softcomputing technique) and which comprises a genetic algorithm assisted by an artificial neural network. The genetic algorithm tries to find the optimal solution by investigating several catalysts (so-called generation) simultaneously. Each successive cat-

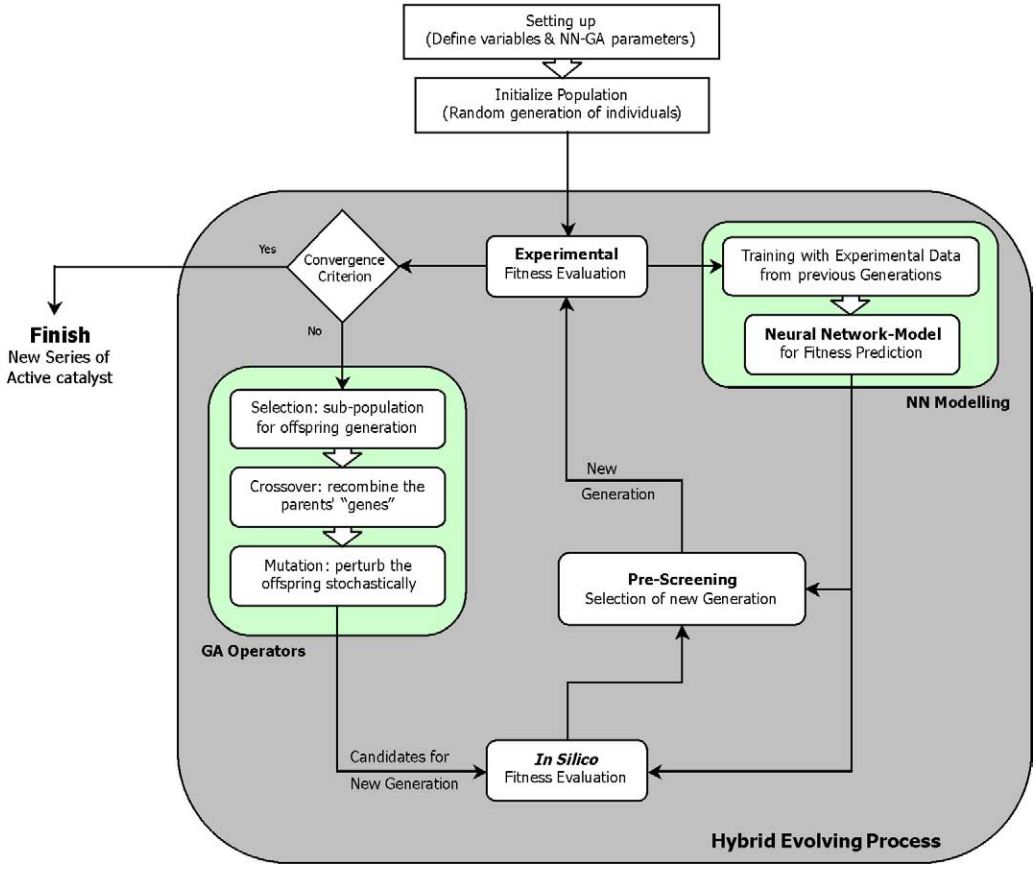

Fig. 3. Scheme of a hybrid optimisation algorithm comprising a genetic algorithm assisted by an artificial neural network.

alyst generation is designed with the previous experimental results taken into account, with the use of GA-specific operators [29]: selection, crossover, and mutation. Through this Darwinian evolution, good catalytic features (genes) dominate the population, resulting in a marked improvement of the catalyst performance. Neural networks (NN) are a nonlinear system able to model and predict complex multidimensional problems like those found in catalysis by high-throughput experimentation [7,30]. In this proposal, the softcomputing algorithm can design the next catalyst generation in a more efficient way, employing knowledge of the parameter space, which was extracted from the NN-modelling of all previous experimental data (previous generations). Fig. 3 shows a simple representation of the operation process of the NN–GA hybrid algorithm.

We decided to adopt real codification [31] in the genetic algorithm, since each variable belongs to a continuous domain. The parents for the next generation are selected with the *roulette wheel* method. The crossover operator is based on confidence intervals [32], which are calculated [33] from the information from the best individuals of the population and predictions of the NN-model. This type of crossover uses procedures that try to promote not only the survival of the best-performing catalysts, but also the survival of those that are both quite fit and different from others, in order to maintain the population diversity. In this way, a new generation is created by the application of crossover and mutation operators with a certain probability. Afterwards, each new generation is evaluated in silico with the NN-based prediction model, and this information is used to obtain a predicted quality rank of catalysts, ordered by fitness function value. Subsequently, a pre-screening of the statistically poor materials is carried out. This final new generation is then experimentally evaluated (synthesised and tested for epoxidation).

This softcomputing method was previously analysed with the use of a hypothetical model in order to maximise the algorithm performance [33,34]. The following aspects were intensively studied: (i) analysis of the different parameters of the genetic algorithm; (ii) analysis of the impact of the initial random generation goodness on GA performance; and (iii) a softcomputing model applied to different catalytic reactions, that is, GA was combined with a NN (GA–NN hybrid). The main conclusion from the above is that GA–NN optimisation performance is dependent on the quality of the initial generation. Thus, to improve the behaviour of this softcomputing technique, the initial set of materials is obtained with a process that guarantees population diversity. This process consists of creating several random generations and carrying out a statistical population study in order to select the most diverse population. The diversity in the initial generation ensures that the optimisation process gains information for the whole search space.

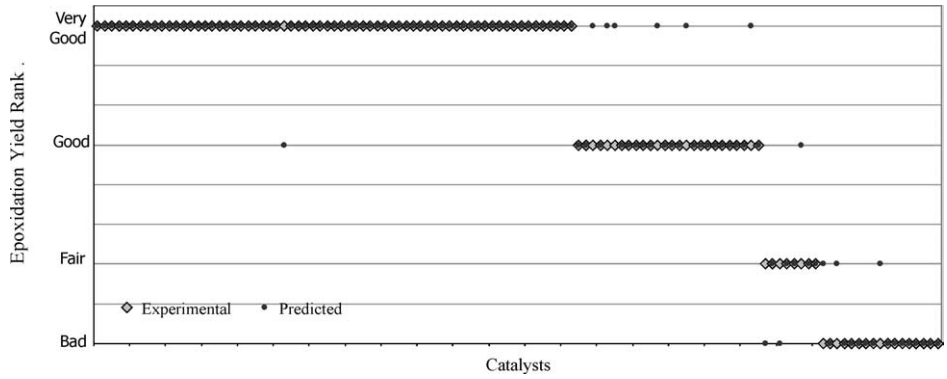

Fig. 4. Prediction performance of the Neural Network Model trained with data derived from the optimisation process of epoxidation catalysts (three generations).

An initial random generation of 38 samples was used to determine an ANN model, after the study of several topologies and training algorithms. In this case, a multilayer perceptron, with four input nodes, two nodes in the first hidden layer, one node in the second hidden layer, and two output nodes, trained with the Backpropagation algorithm with Momentum (learning factor = 0.8 and momentum term = 0.5), was selected. This ANN model was integrated into the sofcomputing algorithm for the design of epoxidation catalysts. After the experimental evaluation of a new generation, the NN-model was retrained with the new available data. If the prediction performance of the NN-model was improved, this retrained model was used in further GA–NN operations; otherwise the previous NN-model was kept. Fig. 4 illustrates the prediction performance achieved by the employed neural network trained with data from three successive generations; that is, the ANN-model makes it possible to predict qualitatively the epoxidation performance of the different catalysts with a certain probability. It is feasible with this model to distinguish a priori between bad-fair and good-very good catalysts.

4. Definition of the materials synthesis space to be explored

Starting gel compositions of mesoporous materials containing titanium are screened in order to optimise the catalytic activity and selectivity in the epoxidation of cyclohexene with *tert*-butyl hydroperoxide as the oxidant. We have selected four synthesis variables (gel compositions) for the optimisation procedure: (i) pH of the gel, (ii) surfactant I (CTMA) content in the gel, (iii) surfactant II (TMA) content in the gel, and (iv) titanium content. Table 1 shows the range of values for each parameter. The other experimental parameters were fixed values established by preliminary studies. The selected objective function was the epoxide yield obtained at 333 K after 5 h of reaction time.

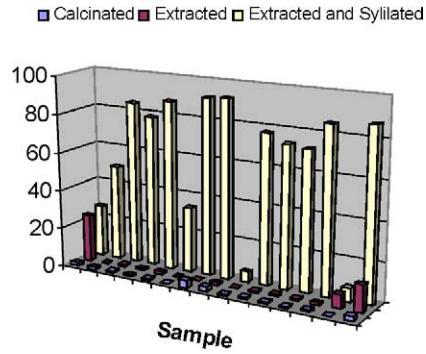

Fig. 5. Effect of post-synthesis treatment in catalytic performance of some Ti-silicate samples in the first catalyst generation. (333 K; 5 h; 785 mg of cyclohexene, 215 mg of TBHP and 5 mg of catalyst).

5. Results and discussion

5.1. Exploration and optimisation process

To evaluate the influence of the postsynthesis treatment on the final catalytic activity, 15 samples of the first generation were subjected in parallel to the three following treatments: (i) calcination (813 K for 6 h), (ii) surfactant extraction, and (iii) extraction and silylation. Calcined and extracted-only materials showed a lower epoxidation activity (Fig. 5) due to fast deactivation by formation and deposition of diols on Ti sites. In this case, diol formation by reaction with water is especially visible, since the water content in the reactor is 1.5 wt%. Meanwhile, extracted and silylated materials exhibited high yields and selectivities towards epoxide ($\sim$ 100%) and *tert*-butylhydroperoxide ($>$ 95%) [35–37]. Therefore, the further optimisation procedure included only

Table 1
Range of parameters explored in the optimisation, i.e., starting gel molar ratios

	Min	Max
CTMA/(Si + Ti)	0.15	0.45
TMA/(Si + Ti)	0.00	0.75
OH/(Si + Ti)	0.15	0.60
Ti/(Si + Ti)	0.001	0.206

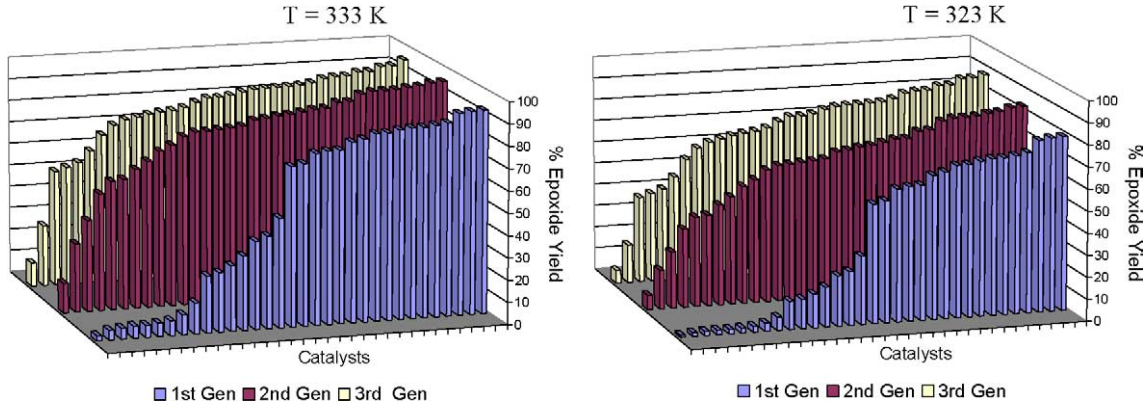

Fig. 6. Epoxidation catalytic performance (epoxide yield) for the three evolved generations at two temperatures (5 h; 785 mg of cyclohexene, 215 mg of TBHP and 5 mg of catalyst).

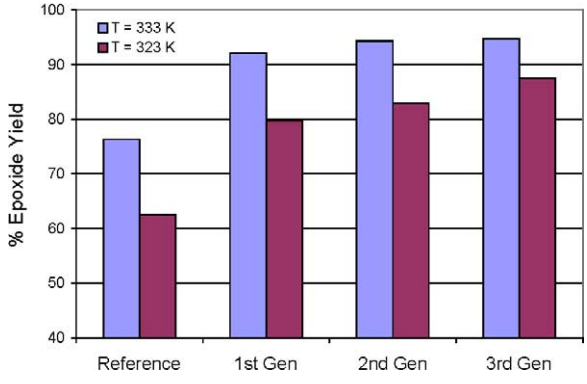

Fig. 7. Influence of temperature for the reference catalyst and best-ranked materials of each generation.

materials subjected to extraction and silylation. In all cases, the mass balance was > 95%.

Three generations of 38 samples have been synthesised and tested. Through the NN–GA optimisation process, an important improvement in the activity and selectivity of the starting materials has been achieved. Fig. 6 shows the cyclohexene epoxide yields obtained for the three consecutive generations (3 × 38 samples) at two different reaction temperatures (323 and 333 K) ordered by increasing yield at 5 h of reaction time. Moreover, the best catalyst found in the last generation strongly improves the rate of epoxidation yield at 323 K with respect to the reference catalyst. The epoxide yield of the best catalyst in each generation and the reference catalyst are compared in Fig. 7, showing the progressive improvement of the epoxidation catalysts, especially when compared at 323 K. With the use of a first-order kinetic model it was possible to calculate a fivefold improvement of the activity of the best catalyst in this study with respect to the reference catalyst [27].

5.2. *Validation of the best Ti-MCM-41 catalysts: epoxidation of linear olefins*

Best-performing catalysts in each generation were tested for epoxidation of different linear olefins, such as 1-hexene, 1-decene, and 1-dodecene. The experiments with linear alkenes were carried out at 333 K, under the same experimental conditions used for cyclohexene epoxidation, that is, a molar olefin/oxidant ratio of 4 and 0.5 wt% of catalyst. The epoxidation rate of these linear olefins is lower than that observed for cyclohexene epoxidation, and, consequently, differences in activity between the different catalysts will be more obvious. The same order of activity that was obtained through the optimisation procedure is observed for the three olefins, and the epoxide selectivity was always very high (∼ 100%). Fig. 8 represents the conversions versus reaction time for 1-hexene, 1-decene, and 1-dodecene, for the reference catalyst and the best catalyst in each generation. A marked enhancement of epoxidation activity achieved with the softcomputing strategy can be observed. Indeed, Table 2 shows the initial reaction rate for epoxidation of the different olefins. It is possible to see there that the initial rate strongly improves from the first to the third catalyst generation, regardless of the reacted olefin.

Table 2
Initial molar rate of epoxide conversion using different olefins

	Initial molar rate (mmol/(g_{cat} h))				
	Structure	Cyclohexene	1-Hexene	1-Decene	1-Dodecene
Reference	MCM-41	0.311	0.013	0.008	0.009
1st generation	MCM-41	0.576	0.031	0.020	0.020
2nd generation	MCM-41	0.849	0.045	0.029	0.030
3rd generation	MCM-41	0.977	0.063	0.046	0.044

Olefin/oxidant molar ratio = 4; reaction temperature, 333 K; 5 mg of catalyst/g feed; and 1.5% H_2O.

Results given in Fig. 9 (epoxide yield at 10 h of reaction time) also show that for all catalysts the order of activity follows the sequence cyclohexene > 1-hexene > 1-decene ≈ 1-dodecene. Since the reactivity of the terminal double C–C bond in these linear olefins should be similar and the diameter of the mesoporous Ti-silicates should not present diffusional limitations, we believe that the small differences in reactivity between the three lineal olefins are related to differences in the adsorption constants of these molecules at the reaction temperature.

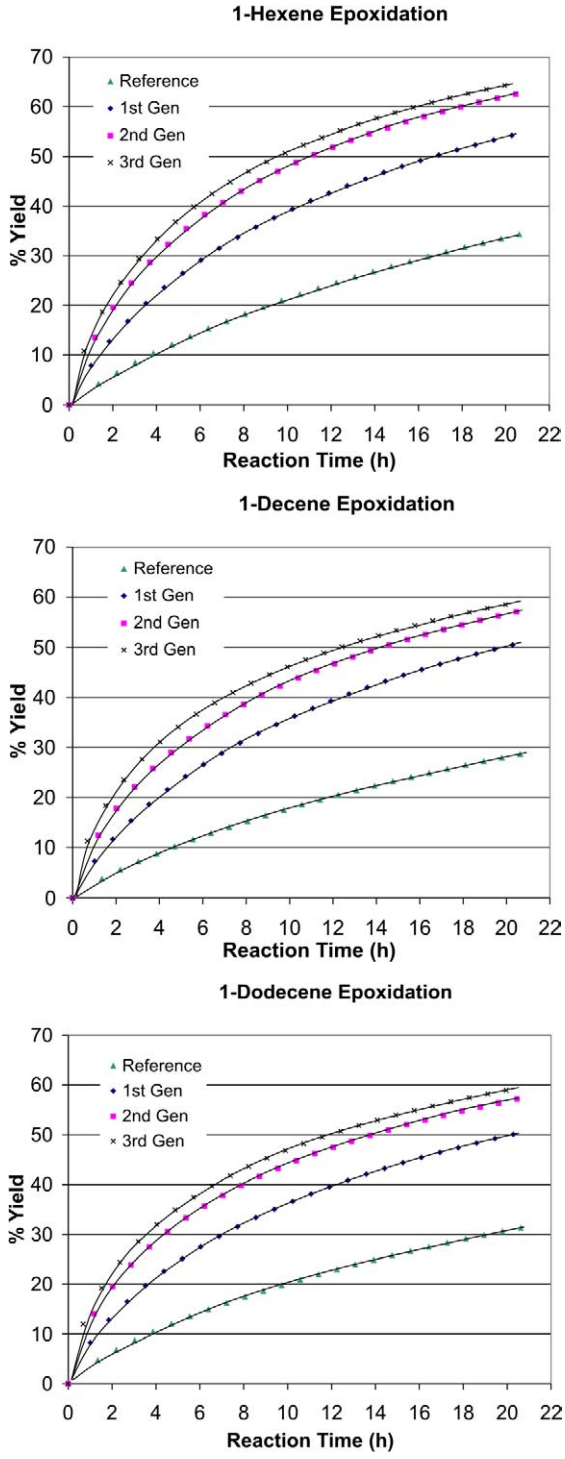

Fig. 8. Epoxide yield evolution for different olefins (1-hexene, 1-decene, and 1-dodecene) over the best-performing catalyst of each generation and the reference catalyst (333 K; 785 mg of olefin, 215 mg of TBHP and 5 mg of catalyst).

5.3. Clustering analysis of experimental data

It is of interest to correlate catalyst synthesis with catalytic results in order to understand how the genetic algorithm works and to extract global conclusions from the ex-

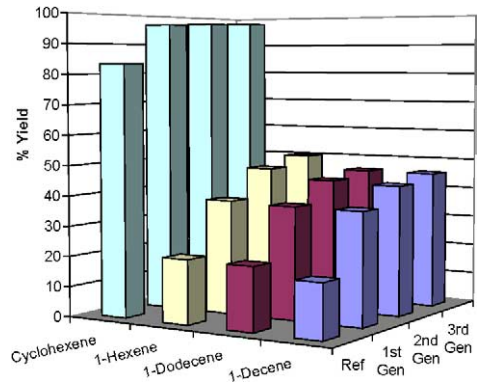

Fig. 9. Catalytic performance of the best-performing catalyst of each generation and reference catalyst, using cyclohexene, 1-hexene, 1-decene, and 1-dodecene as substrates (333 K; 10 h; 785 mg of olefin, 215 mg of TBHP and 5 mg of catalyst).

periments. The large number of samples and the multidimensional space data ([CTMA], [TMA], [OH], and [Ti]) do not allow an exhaustive analysis of each result, but nevertheless some general tendencies can be extracted for cyclohexene epoxidation at 333 K. Fig. 10 shows the distribution by pairs of the different synthesis variables for all catalysts as a function of their epoxidation performance. Thus, catalysts have been classified into three groups according to their epoxide yield: (a) high active materials, $> 90\%$; (b) middle active materials, 60–90%; and (c) low active materials, $< 60\%$.

In Fig. 10, several areas can be distinguished by the probability of finding different levels of activity, and catalysts with activities higher than the reference catalyst (78%) were found in a wide range of gel compositions. However, the best activities were found around two clusters of [TMA], [CTMA], [OH], and [Ti] concentrations. Good performances have been achieved for a $\mathrm{CTMA}/(\mathrm{SiO_2} + \mathrm{Ti})$ molar ratio between 0.15 and 0.42. Similar conclusions can be extracted for Ti contents, with a maximum epoxide yield between $\mathrm{Ti}/(\mathrm{SiO_2} + \mathrm{Ti})$ molar ratios of 0.012 and 0.061. In relation to [OH], we have not found satisfactory performances above a $\mathrm{OH^-}/(\mathrm{SiO_2} + \mathrm{Ti})$ molar ratio of 0.27, and this factor seems to be crucial. The best results with TMA have been obtained under 0.1 $\mathrm{mol}/(\mathrm{SiO_2} + \mathrm{Ti})$, in spite of the fact that some samples with higher TMA values and low values of $\mathrm{OH^-}$ can give yields near 80%. The reference catalyst presents Ti and $\mathrm{OH^-}$ values inside the maximum activity cluster, but with less CTMA and more TMA than for the global maximum found. The results presented here clearly show that it should be possible to achieve high activity and selectivity for a very low level of TMA or even without introduction of TMA in the synthesis media, provided that an adequate pH is achieved by means of CTMA. This is an important finding since it makes it possible to decrease the synthesis cost of the mesoporous Ti-silicates.

5.4. Characterisation

XRD measurements showed that from a crystallographic point of view, three types of materials are occurring in the

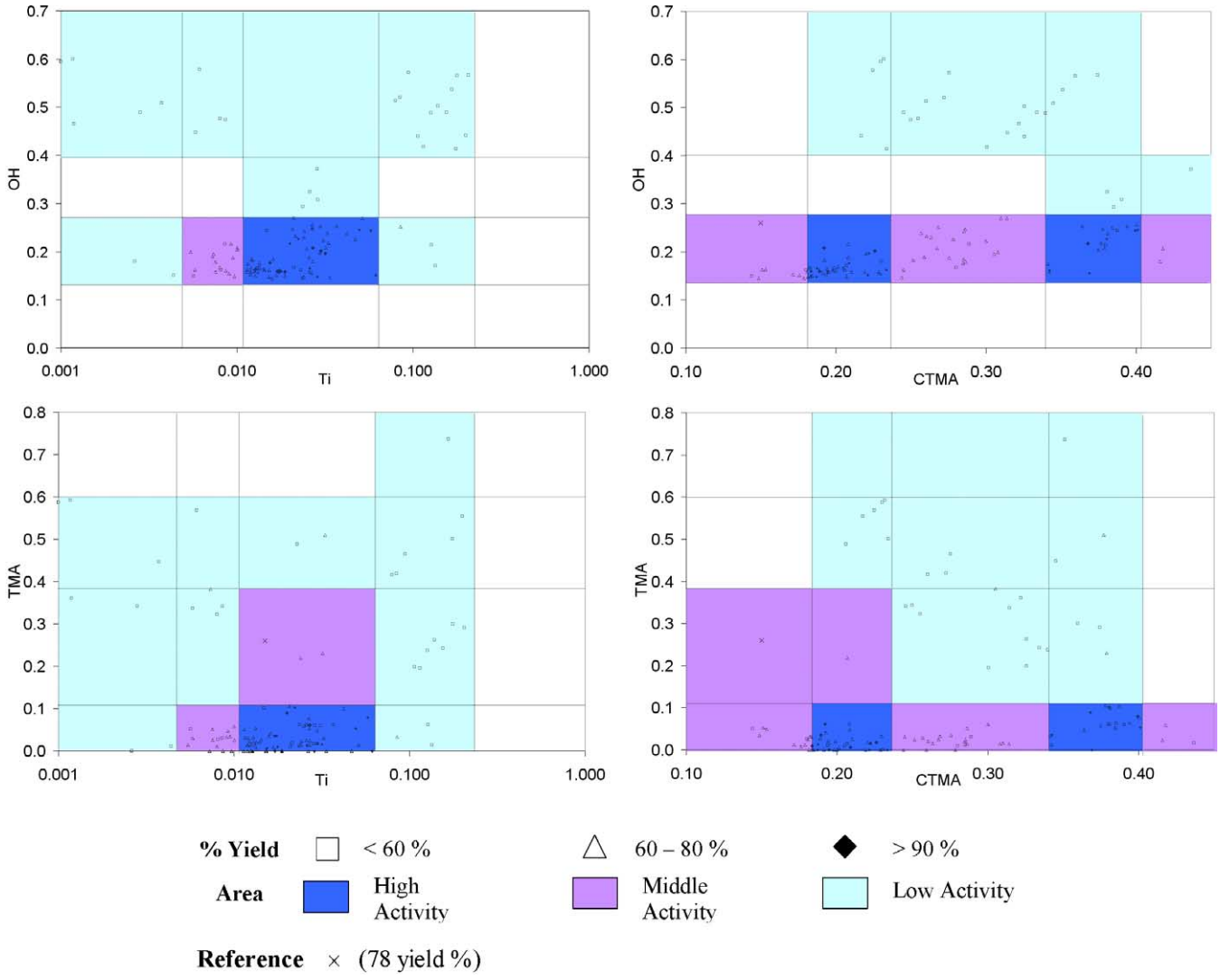

Fig. 10. Clustering analysis showing the relationships between synthesis variables by pairs and epoxidation performance at 333 K for the catalysts of the three evolved generations. Experimental space has been partitioned into different activity-level areas (clusters).

explored space, that is, MCM-41 and MCM-48 with different degrees of structure order, and a low ordered material. Fig. 1 shows the diffractograms obtained with the selected samples, including the best performing catalysts and some samples representing defined regions of the explored space (samples 1–20). Samples with $OH^-/(SiO_2 + Ti)$ molar ratios above 0.27 have not been studied by XRD because of their low activity and the poor synthesis yield. We grouped the diffractograms obtained, taking into account the type of material and the level of structure order. It is possible to find well-ordered MCM-41 and MCM-48 samples, lower ordered MCM-41 samples, and one material with low structure order. Fig. 12 shows the distribution of materials along the data space. MCM-48 materials have been obtained only in a reduced composition area, whereas MCM-41 can be observed in a wide range of values. MCM-48 requires high values of CTMA and OH and low values of TMA, in agreement with [24]. On the other hand, well-ordered MCM-41 has been achieved only with Ti values under 0.018 $Ti/(SiO_2 + Ti)$, but in a wide range of CTMA, OH, and TMA (even with low TMA and OH). With regard to MCM-41 samples, different pore sizes have been obtained, as can be concluded from the variation in the first reflection angle [38] (from sample 8 = 1.86 to sample 7 = 2.46). As can be observed in Fig. 13, the MCM-41 pore size can be related to gel compositions: the higher the organic content in the gel (CTM + TMA), the higher the pore diameter. SEM imaging of different high-activity samples (Table 3) showed that materials with diverse particle size are occurring in the explored space, from the nanoscale (< 0.1 μm) to the microscale (> 1 μm).

Although different mesoporous structures were found that which are catalytically active (Table 3), there is not a direct relationship between the type and order of the structures and catalytic activity. Cyclohexene epoxide yields higher than 90% have been achieved with both MCM-41 and MCM-48. In addition, high epoxide yields (> 80%) have been obtained even with less ordered Ti-MCM-41 materi-

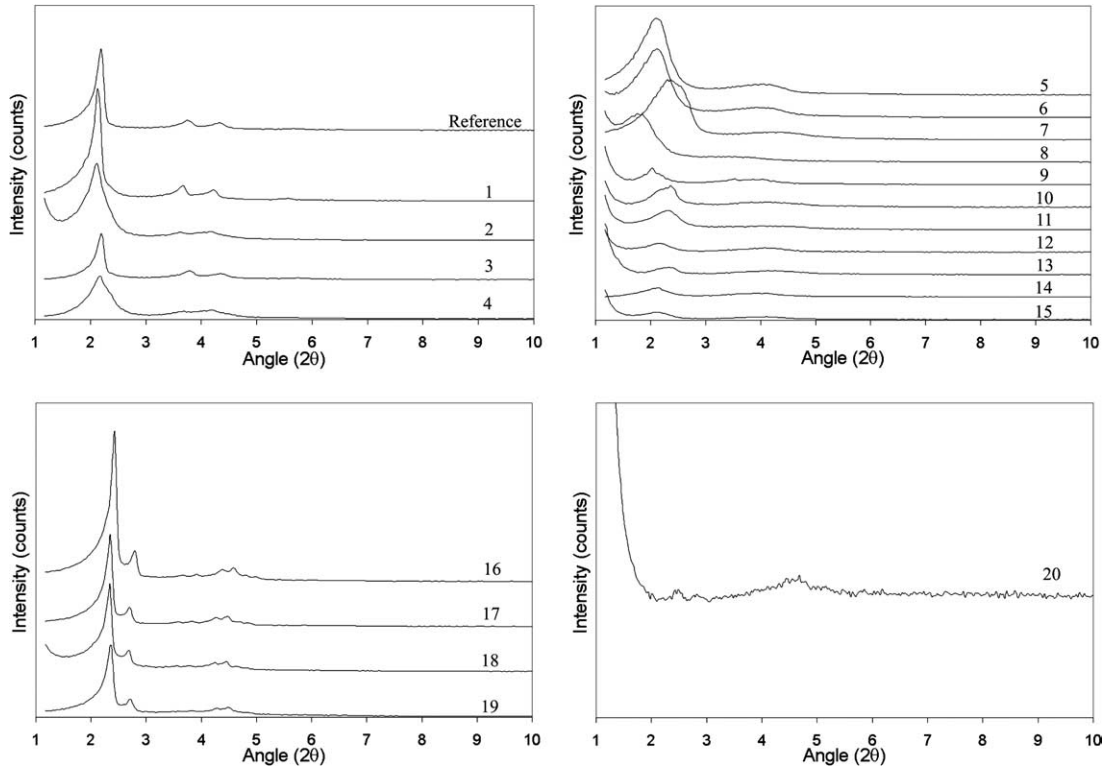

Fig. 11. XDR patterns of representative synthesis samples: well-ordered MCM-41 (left top); poor-ordered MCM-41 (right top); well-ordered MCM-48 (left bottom), and an apparently amorphous Ti-silicate (right bottom).

Table 3
Main structure characteristics of best-performing samples. High activity has been obtained with well-ordered and poor ordered MCM-41, well-ordered MCM-48 and amorphous Ti-Silicate

Sample	Synthesis	Testing	XRD		UV–vis DRS		Elemental analysis	SEM images
	$Ti/(Ti + SiO_2)$	Epoxide yield (%)	Structure	Structure order	λTi^{IV}	Area ratio[a]	C content (wt%)	Crystal size (μm)
7	0.032	94.7	MCM-41	Low order small pore size	213	6.9	13.42	0.15–0.25
5	0.017	94.6	MCM-41	Low order	215	12.0	12.39	0.08–0.12
2	0.018	92.9	MCM-41	High order	211	15.0	11.93	0.1–0.2
15	0.061	92.1	MCM-41	Low order	217	3.6	11.44	0.5–1.5
18	0.049	91.2	MCM-48	High order	215	7.9	11.73	0.4–0.5
13	0.027	90.8	MCM-41	Low order	212	13.1	12.76	0.2–0.4
6	0.017	90.1	MCM-41	Low order	214	9.3	11.41	0.08–0.12
17	0.024	88.2	MCM-48	High order	213	7.0	12.15	0.5–2
20	0.085	85.2	–	Very low order	220	4.2	9.42	0.05–0.3
Reference	0.015	76.3	MCM-41	High order	216	16.0	11.42	7–15

[a] Ratio between the area band at 215 ± 5 nm and the area band at 270 nm.

als. However, it should be noticed that the sample with low structure order, while more active than the reference catalyst, is less active than the Ti-MCM-41 optimised samples with medium and high crystallinities.

The coordination of titanium was studied by DR–UV spectroscopy. Fig. 14 shows UV–vis DRS spectra for samples 1 to 20. One intense band at 215 ± 5 nm can be observed, which can be assigned to tetrahedral titanium sites, together with an important shoulder at ~ 270 nm. It is known [23,26,27] that extracted and silylated Ti-silicates have enough hydrophobicity to impede coordination of water with Ti, so the band at ~ 270 nm will probably correspond to partially polymerised hexacoordinated Ti species. Even when the other synthesis parameters are varied over a wide range, it can be observed that when the titanium content in the gel is increased, the presence of polymeric titanium species increases (270 nm), whereas the order of the mesoporous structures decreases. We made a deconvolution analysis of the UV–vis DRS bands by fitting the original spectrum to two Gaussian peaks centred at 215 ± 5 and 270 nm. Table 3 shows the Ti content in some interesting high-activity samples and the UV–vis peak deconvolution. In Fig. 15, the wavelength for the adsorption of Ti and the ratio of the areas of the bands at ~ 215 nm and 270 nm in

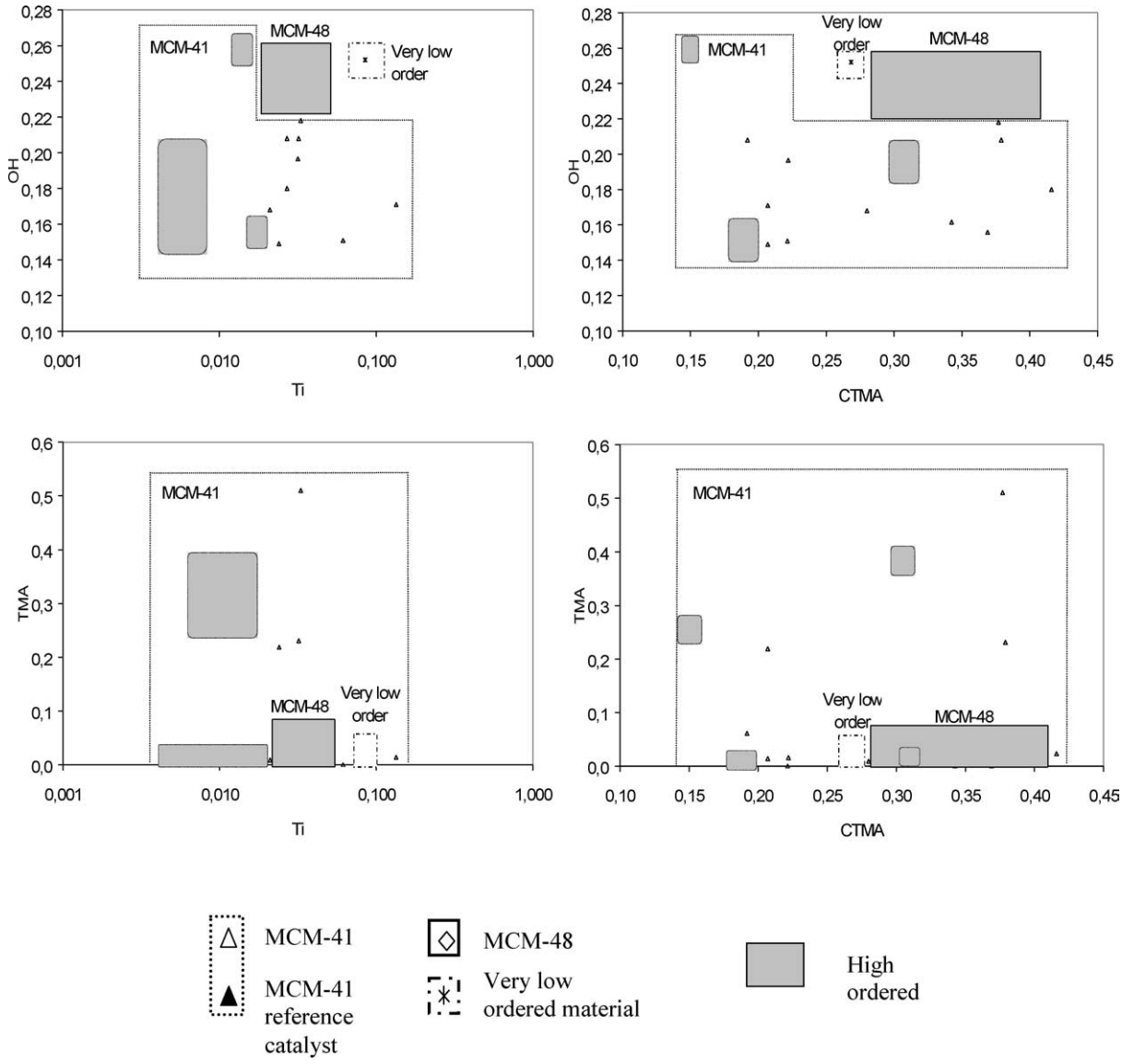

Fig. 12. Mapping of the different materials obtained among 20 representative samples. MCM-41 with different degrees of structure order, MCM-48 and an apparently amorphous material can be observed.

samples with different contents have been plotted. A direct relationship between the titanium content and the amount of polymeric titanium species can be seen. It should be taken into account that the rest of the synthesis variables also seem to influence the final distribution of titanium, and this can explain the dispersion observed in Fig. 15. The highest catalytic activity has been achieved with the introduction of a large amount of Ti (0.032, double the amount of the reference catalyst), and even higher levels of Ti (until 0,085) can be present with excellent catalytic results. However, the composition of certain samples also allows satisfactory performances with low Ti contents, and we have obtained epoxide yields of 88% with a $Ti/(SiO_2 + Ti)$ ratio of only 0.006.

Table 3 shows the measured carbon content introduced by the silylation process and gives an idea of the hydrophobicity of the surface of materials; that is, the higher the silylation level, the more hydrophobic will be the resultant sample [22]. It can be seen that active materials have a very

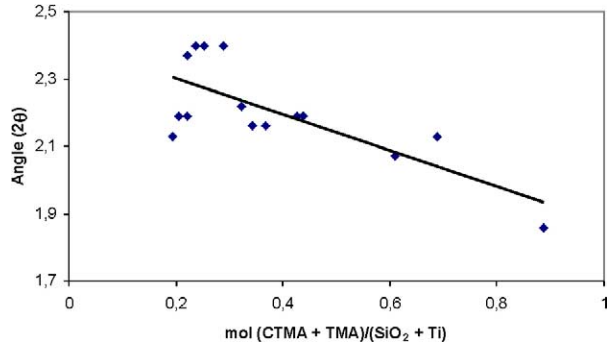

Fig. 13. Relationship between surfactant content and the first reflection angle of MCM-41 samples. In general, high quantities of CTMA and TMA lead to materials with larger pores (lower first reflection angles).

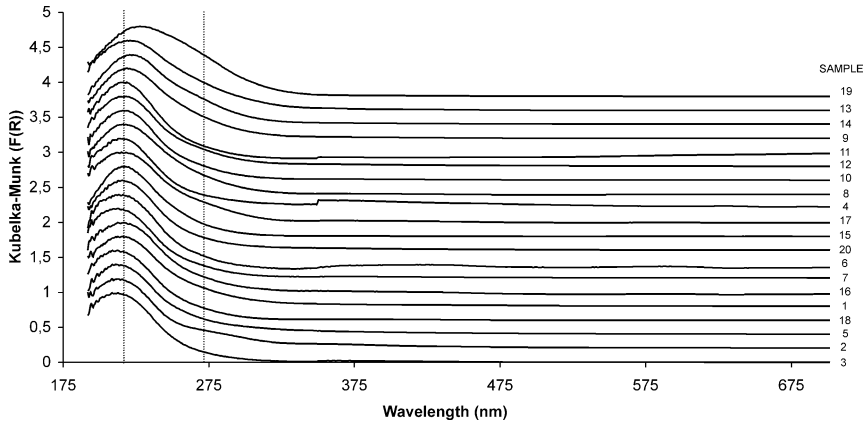

Fig. 14. UV–vis DRS spectra of some representative Ti-silicate materials.

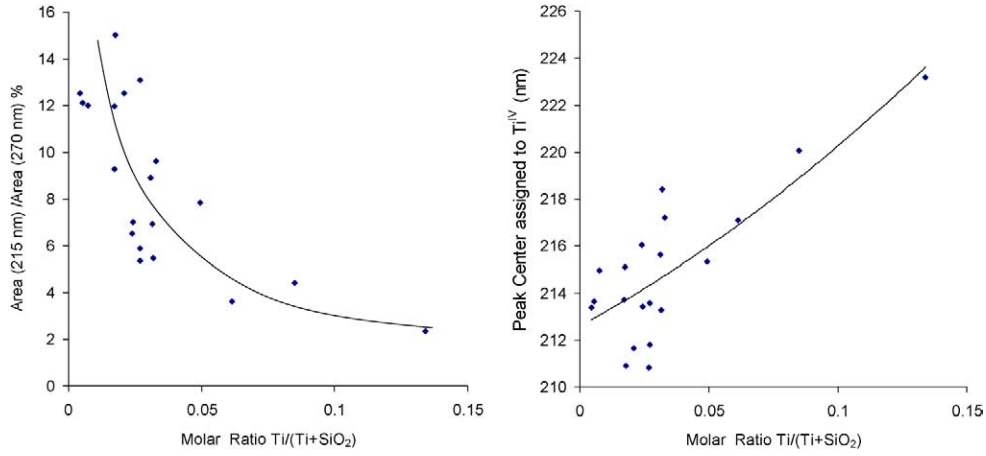

Fig. 15. Relationship between the area of UV–vis DRS peaks (215 ± 5 and 270 nm) and Ti synthesis content. UV–vis DRS spectra were analysed by deconvolution of two Gaussian peaks with maximum at 215 ± 5 and 270 nm. In general, higher Ti contents produces less tetrahedral titanium (215 ± 5 nm) and more polymeric titanium (270 nm). Polynomial fitted lines are introduced for better trend visualization.

high content of carbon, and the most active samples have the highest carbon content.

6. Conclusions

Through the optimisation process, two types of mesoporous Ti-silicate materials with enhanced epoxidation activity and selectivity have been found. The strategy for the experimental design has made it possible to explore the multidimensional space and optimise the areas exhibiting the highest epoxidation performances. Thus, this model study has allowed us to study simultaneously the four synthesis variables (reactant concentrations) and to map the nonlinear space. HT synthesis and catalytic testing were accompanied by conventional characterisation, allowing us to discuss the catalytic results obtained in terms of material structure, that is, Ti coordination, nature of the active sites, and hydrophobicity of the catalyst surface. By means of clustering and factorial analysis of the multiparametric results, it was possible to correlate gel composition with catalytic activity, Ti-silicate structure, and coordination of Ti sites.

This work shows an integrated application of high-throughput experimentation tools with advanced optimisation algorithms for experimental design. The high-speed experimentation was guided by artificial intelligent techniques, that is, a hybrid algorithm consisting of a GA coupled with a neural network. This hybrid system seems to be a new useful tool for the intelligent discovery of new catalytic materials, since it has appropriate tools for high-dimensional optimisation while it can keep in memory the whole “history” of the search, reducing the screening of statistically poor active materials.

Acknowledgments

Financial support by Spanish MAT2003-07945-C02-01, TIC2003-07369-C02-01, and CICYT DPI2002-04434-C04-02 and EU Project TOPCOMBI and grants FPU AP2001-1516 and FPU AP2003-4635 is gratefully acknowledged. Moreover, the authors thank J.L. Jordá for discussion and I. Millet for technical assistance.

References

[1] Montgomery, Design and Analysis of Experiments, Wiley, New York, 2001.
[2] L. Végvári, A. Tomposb, S. Gobölös b, J. Margitfalvi, Catal. Today 81 (3) (2003) 517–527.
[3] J. Klein, T.Z. Ech, J.M. Newsam, S.A. Schunk, Appl. Catal. 254 (1) (2003) 121–131.
[4] M.A. Aramendía, V. Borau, C. Jiménez, J.M. Marinas, F.J. Romero, F.J. Urbano, J. Catal. 209 (2) (2002) 413–416.
[5] O. Buyevskaya, D. Wolf, M. Baerns, Catal. Today 200 (2000) 63–67.
[6] J.M. Serra, A. Chica, A. Corma, App. Catal. A 239 (2003) 35–42.
[7] A. Corma, J.M. Serra, E. Argente, S. Valero, V. Botti, Chem. Phys. Chem. 3 (2002) 939–945.
[8] C. Klanner, D. Farrusseng, L. Baumes, C. Mirodatos, F. Schueth, QSAR & Comb. Sci. 22 (7) (2003) 729–736.
[9] F. Gilardoni, A. Graham, B. McKay, B. Brown, in: Proceedings of 225th ACS National Meeting, New Orleans (USA), 23–27 March 2003.
[10] L. Baumes, D. Farrusseng, M. Lengliz, C. Mirodatos, Using Artificial Neural Networks to boost high-throughput discovery in heterogeneous catalysis, QSAR & Combinatorial Science, in press.
[11] D. Farrusseng, L. Baumes, C. Mirodatos, in: R.A. Potyrailo, E.J. Amis (Eds.), High-Throughput Analysis: A Tool For Combinatorial Materials Science, Kluwer-Academic/Plenum, 2003, pp. 551–579.
[12] C. Klanner, D. Farrusseng, L. Baumes, C. Mirodatos, F. Schueth, Angew. Chem. Int. Ed. 43 (2004) 5347–5349.
[13] L. Zadeh, Commun. ACM 37 (1994) 939–945.
[14] S.B. Cho, Integ. Comput.-Aid. Eng. 9 (2002) 363–372.
[15] M. Taramasso, G. Perego, B. Notari, US Patent 4410501 (1983), to Snambrogetti S.p.A.
[16] D.R.C. Huybrechts, L. DeBruycker, P.A. Jacobs, Nature 345 (1990) 240.
[17] A. Corma, P. Esteve, A. Martinez, J. Catal. 161 (1996) 11.
[18] A. Corma, L. Nemeth, M. Renz, S. Valencia, Nature 412 (2001) 423–425.
[19] A. Corma, V. Fornés, S. Iborra, M. Mifsud, M. Renz, J. Catal. 221 (1) (2004) 67–76.
[20] S. Imamura, T. Nakai, H. Kanai, T. Ito, Catal. Lett. 28 (2–4) (1994) 277–282.
[21] A. Corma, F. Rey, M.E. Domine, M. Peña, WO0044670 (1994), to UPV-CSIC.
[22] A. Corma, J.L. Jordá, M.T. Navarro, F. Rey, Chem. Comm. (1998) 1899–1900.
[23] M.L. Peña, Q. Kan, A. Corma, F. Rey, Micropor. Mesopor. Mater. 44–45 (2001) 345–356.
[24] M.L. Peña, Q. Kan, A. Corma, F. Rey, Micropor. Mesopor. Mater. 44–45 (2001) 9–16.
[25] T. Tatsumi, K.A. Koyano, N. Igarashi, Chem. Comm. (1988) 325.
[26] T. Blasco, M.A. Camblor, A. Corma, P. Esteve, J.M. Guil, A. Martínez, J.A. Perdigón, S. Valencia, J. Phys. Chem. B 102 (1998) 75.
[27] A. Corma, M. Domine, J.A. Gaona, J.L. Jordá, M.T. Navarro, F. Rey, J. Pérez-Pariente, J. Tsuji, B. McCullock, L.T. Nemeth, Chem. Comm. (1998) 2211.
[28] T. Blasco, A. Corma, M.T. Navarro, J. Pérez-Pariente, J. Catal. 156 (1995) 65–74.
[29] L. Goldberg, Genetic Algorithms in Search, Optimization and Machine Learning, Addison–Wesley, Boston, 1989.
[30] K. Huang, F.Q. Chen, D.W. Lü, Appl. Catal. A 219 (2001) 61–68.
[31] R.C. Rowe, R.J. Roberts, in: Intelligent Software for Product Formulation, Taylor and Francis, London, 1998.
[32] D. Ortiz, C. Hervás, J. Munoz, in: ESANN 2001, Bruges, Belgium, 2001, pp. 193–198.
[33] S. Valero, E. Argente, V. Botti, J.M. Serra, A. Corma, in: E. Conejo, M. Urretavizcaya, J.L. Perez-de-la-Cruz (Eds.), Current Topics in Artificial Intelligence, vol. 3040, Springer, Heidelberg, 2004, pp. 536–545.
[34] S. Valero, E. Argente, J.M. Serra, P. Serna, V. Botti, A. Corma, in: R. López, L. Saitta (Eds.), Proceedings of European Conference on Artificial Intelligence, Amsterdam, IOS Press, 2004, pp. 765–769.
[35] M.A. Camblor, A. Corma, P. Esteve, A. Martínez, S. Valencia, Chem. Comm. (1997) 795.
[36] K.A. Koyano, T. Tatsumi, Y. Tanaka, S. Nakata, J. Phys. Chem. 101 (1997) 9436.
[37] J. Liu, X. Feng, G.E. Fryxell, L.Q. Wang, A.Y. Kim, M. Gong, Adv. Mater. 10 (1998) 161.
[38] J.S. Choi, D.J. Kim, S.H. Chang, W.S. Ahn, Appl. Catal. A 254 (2003) 225–237.